THE JOURNAL OF PHYSICAL CHEMISTRY Letters

Letter

pubs.acs.org/JPCL

Dynamic Charge Storage in Ionic Liquids-Filled Nanopores: Insight from a Computational Cyclic Voltammetry Study

Yadong He,[†] Jingsong Huang,[‡] Bobby G. Sumpter,[‡] Alexei A. Kornyshev,[¶] and Rui Qiao*,[†]

[†]Department of Mechanical Engineering, Virginia Tech, Blacksburg, Virginia 24061, United States

[‡]Center for Nanophase Materials Sciences and Computer Science & Mathematics Division, Oak Ridge National Laboratory, Bethel Valley Road, Oak Ridge, Tennessee 37831, United States

[¶]Department of Chemistry, Faculty of Natural Sciences, Imperial College London, SW7 2AZ London, United Kingdom

Supporting Information

ABSTRACT: Understanding the dynamic charge storage in nanoporous electrodes with room-temperature ionic liquid electrolytes is essential for optimizing them to achieve supercapacitors with high energy and power densities. Herein, we report coarse-grained molecular dynamics simulations of the cyclic voltammetry of supercapacitors featuring subnanometer pores and model ionic liquids. We show that the cyclic charging and discharging of nanopores are governed by the interplay between the external field-driven ion transport and the sloshing dynamics of ions inside of the pore. The ion occupancy along the pore length depends strongly on the scan rate and varies cyclically during charging/discharging. Unlike that at equilibrium conditions or low scan rates, charge storage at high scan rates is dominated by counterions while the contribution by co-ions is marginal or negative. These observations help explain the perm-selective charge storage observed experimentally. We clarify the mechanisms underlying these dynamic phenomena and quantify their effects on the efficiency of the dynamic charge storage in nanopores.

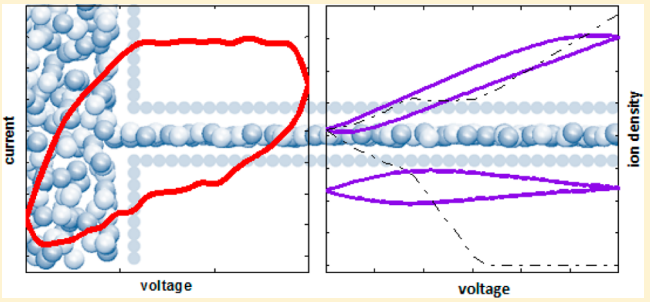

Supercapacitors have gained considerable attention in recent years due to their distinct advantages such as high power density, safety, and extraordinary cycle life. The widespread deployment of supercapacitors, however, is hindered by their moderate energy density.[1] There is an emerging consensus that porous carbon electrodes with subnanometer pores and room-temperature ionic liquid (RTIL) electrolytes, which allow large specific surface area, large specific capacitance, and high operating voltage to be simultaneously integrated in the same device, are among the most promising materials for high energy density supercapacitors.[2,3] These materials, however, are not without limitations. Ion transport in subnanometer pores may be more sluggish compared to that in mesopores and macropores due to the spatial confinement. In addition, some prior experimental studies indicated that supercapacitors based on RTILs have relatively low power density,[4] implying that the energy density of supercapacitors can be compromised at high charging/discharging rates. It is thus important to optimize the performance of supercapacitors utilizing carbon nanopores and RTILs to achieve high energy densities at high charging/discharging rates. This challenge demands a fundamental understanding of the *dynamic* charge storage of supercapacitors based on these promising materials.

Experimental studies of the dynamic charge storage in supercapacitors traditionally relied on cyclic voltammetry, galvanostatic cycling, and so forth, which probe the macroscopic electrochemical performance. In comparison, the application of powerful techniques such as the electrochemical quartz crystal microbalance (EQCM),[5,6] NMR spectroscopy,[7] and infrared spectroelectrochemical techniques[8] may provide molecular information about the dynamic charge storage. For example, using an in situ infrared spectroelectrochemical technique in conjunction with cyclic voltammetry, Richey et al. provided direct evidence for ions entering and exiting electrode nanopores immersed in RTILs during charging/discharging.[8] Using EQCM, Tsai et al. revealed that at high polarization, counterions dominate the charge storage in carbide-derived carbon (CDC) electrodes immersed in 1-ethyl-3-methylimidazolium-bis(trifluoromethylsulfonyl)imide (EMI-TFSI) ionic liquid.[9] These studies provided unprecedented details on the dynamic charge storage in supercapacitors at the electrode level, that is, an ensemble average of all pores inside of electrodes. However, the charging dynamics in individual pores, especially the underlying ion dynamics along the pore length, was not resolved in these experimental works. In addition to these limitations, some intriguing phenomena revealed in these studies (e.g., the predominance of counterions in charge storage inside narrow pores) are yet to be fully rationalized. These issues highlight that significant gaps still remain in the understanding of the dynamic charge storage in

Received: November 17, 2014
Accepted: December 4, 2014

   dx.doi.org/10.1021/jz5024306 | J. Phys. Chem. Lett. 2015, 6, 22−30

nanopores filled with RTILs. Filling such a knowledge gap is essential for the rational design of nanoporous electrodes and RTIL electrolytes for optimal dynamic charge storage. Computer simulations, especially those at the single-pore level, may lend critical insight by spatially and temporally resolving the dynamic charge storage.

At present, only a limited number of computer simulations of the charging dynamics in subnanometer pores exist. The first such simulation,[10] based on a mean-field phenomenological model, suggested that the charging of a pore prewetted by RTILs is a diffusive process. This prediction has been confirmed in recent molecular dynamics (MD) simulations.[11] Although the diffusive nature of charging revealed by these simulations is in apparent agreement with the transmission line model (TLM), the physics underlying the time constant of charging differ fundamentally from that in the TLM.[11] In addition, these MD simulations using simplistic models for ions and pores indicated that the charging of subnanometer pores is fast: the ion diffusion inside a pore *during charging* can be very fast despite geometrical confinement, and the collective transport of ions due to electrical migration greatly accelerates charging. Both the diffusive and fast characteristics found in the charging of subnanometer pores are corroborated by recent MD simulations of the charging of nanoporous electrodes with realistic pore structures.[12] These works suggest that nanoporous electrodes and RTILs can potentially lead to high energy density supercapacitors capable of operating at high charging/discharging rates. Most of these simulations, however, did not study the discharging of nanopores, which is not a simple reversal of the charging process and is critical for understanding the energy efficiency of dynamic charge storage. Furthermore, except for one of the most recent works,[13] all previous studies dealt with the charging of nanopores by impulsively imposed voltages, while nanopores are typically subject to *cyclic* charging/discharging during characterization and in practical operation of supercapacitors.

Here, we perform MD simulations of the cyclic voltammetry of subnanometer pores connected with RTIL reservoirs, which have so far only been studied experimentally but not using molecular simulations. By dissecting the cyclic voltammetry with molecular resolution, we clarify the essential features of the dynamic charge storage in nanopores, its underlying ion dynamics, and how its macroscopic characteristics such as energy density and charge storage efficiency are affected by pore size and voltage scan rates.

The MD simulation system consists of a pair of identical slit pores and RTIL reservoirs (see Figure S1, Supporting Information). The walls of each pore are maintained as ideally polarizable surfaces (see the Methods section). The slit shape of the pore is similar to that found in an emerging class of electrode materials based on graphene and MXene, which feature well-aligned pores with large length-to-width aspect ratios.[14,15] Cations and anions of our model RTILs are nearly spherical and of identical size, and their specific interactions with the pore walls are not taken into account. With these coarse-grained models, we seek to reveal the essential physics of the collective interactions of ions in subnanometer pores and their manifestations in the dynamics of charge storage. The main idea is to discuss these separately from the effects that may be caused by the chemical complexities of RTIL ions and details of interactions of ions with real electrode materials. The effectiveness of these coarse-grained models in delineating the charging dynamics in practical materials is supported by the fact that the key features of charging dynamics predicted using these models[11] are indeed observed in simulations employing more realistic electrode and RTIL models.[12]

Each cyclic voltammetry simulation begins with a pore + reservoir system pre-equilibrated with the voltage between the two pores set to zero, that is, ions in each pore are at the potential of zero charge (PZC) state. Starting at $t = 0$, the voltage difference between the two pores is increased from 0 to the target potential (forward scan) and then decreased to 0 (backward scan), both at the same scan rate of s. These scans are repeated until the system reaches a periodic steady state. We perform simulations in systems with two pore sizes separately (center-to-center width: 0.78 and 0.91 nm) and five scan rates for each pore size (s = 1.88, 3.75, 5, 7.5, and 10 V/ns). These scan rates are orders of magnitude faster than that in common experimental systems with long nanopores. However, as shown later, for the model system studied here, nanopores retain significant charge storage capability even at s = 10V/ns due to their short length and the fast diffusion of our model RTILs. Hence these fast scan rates still allow us to effectively explore the physics of dynamic charge storage in nanopores.

To help understand the cyclic voltammetry results, we first recapitulate the essential features of the thermodynamics and ion transport underlying charge storage in narrow pores. Under quasi-static or equilibrium conditions, these pores store charge very effectively for two reasons. First, ion−ion electrostatic interactions are strongly screened by the pore walls.[16] Second, in pores polarized by a given voltage, the number of co-ions inside of the pore decreases when the pore width reduces, which helps suppress overscreening and "solvation" of ions by ions with opposite charges and thus leads to more effective storage of counterions in narrower pores.[17−22] It is interesting to note that, while both counterion insertion and co-ion removal contribute to charge storage, as manifested by the peak in capacitance−voltage curves, charge storage inside of narrow pores is especially effective when it is achieved mainly by removal of co-ions[23] (also termed demixing of counterions and co-ions[24]).

In addition to the above thermodynamic factors, charge storage is also affected by the transport of ions. In typical supercapacitors, the resistance for the ion transport between the pore entrance and electrolyte reservoir (i.e., separators soaked with electrolytes) is small. Therefore, in response to a change of the electrode polarization, the densities of the counter/co-ions at the pore entrance quickly adjust toward their quasi-static values corresponding to the new voltage. The net transport of ions into/out of the pore is thus throttled by the internal transport of ions toward the pore entrance or interior. For example, during charging, the net flux of counterions into the pore is limited by how fast counterions are transported from the pore entrance toward the pore interior. For ions inside of slit-shaped pores with widths comparable to the ion size, their fluxes, according to a recent mean-field theory, can be given by[10,11]

$$J_{\pm} = -D_{\pm}\nabla\rho_{\pm} \mp D_{\pm}\rho_{\pm}G\nabla q - D_{\pm}\rho_{\pm}/(\rho_{\max} - \rho_{\Sigma})\nabla\rho_{\Sigma} \qquad (1)$$

where $D_{\pm}$ is the ion diffusion coefficient, $\rho_{\pm}$ is the ion density, $q = \rho_{+} - \rho_{-}$ is the ionic charge in units of elementary charge, $\rho_{\Sigma} = \rho_{+} + \rho_{-}$ is the total ion density, and $\rho_{\max}$ is the total ion density at close packing. In eq 1, $G = e^2/\pi\epsilon_{\mathrm{p}}k_{\mathrm{B}}T\sum_{n=1}^{\infty}\sin^2(\pi n/2)K_1(n\pi R_{\mathrm{c}}/L)/n$, where e is the elementary charge, ϵ_{p} is the permittivity inside of the pore, $k_{\mathrm{B}}T$ is the thermal energy, K_1 is the modified Bessel function of the second kind of the first

dx.doi.org/10.1021/jz5024306 | J. Phys. Chem. Lett. 2015, 6, 22−30

order, R_c is the cutoff radius, and L is the pore width.[10] G characterizes electrostatic ion−ion interactions screened by the conducting pore walls. The first term of eq 1 is the diffusion of ions. The second term is the electrical ion migration originating from electrostatic ion−ion interactions, and it often dominates the overall ion transport. The last term denotes the ion transport due to the gradient of the total ion density along the pore. While mechanisms such as ion transport due to hydrodynamic flows and friction between different ion species are not accounted for in this model, eq 1 can provide an effective description of the ion transport in narrow pores, especially when the counterion and co-ion densities do not differ greatly. When the density of counterions inside of a pore far exceeds that of the co-ions, the transport of co-ions approaches simple diffusion.[11]

Equation 1 has two straightforward implications. First, as proved in our recent MD simulations,[11] it suggests that ion transport is more effective in wider pores because G increases as pores become wider. Second, because the migration flux of an ion species is proportional to its density and both counterions and co-ions are driven by the same gradient of ionic charge, eq 1 suggests that the flux of counterions, whose density is always higher than that of the co-ions, is typically higher than that of the co-ions. Trivially, the flux of any ion species inside of the pore tends to be higher when its density is larger. These latter two effects have not yet received significant attention in the study of dynamic charge storage. However, as detailed below, they can play a key role in the intriguing phenomena revealed in recent experimental in-situ studies of ion dynamics in supercapacitors.[8,9]

Initial Transients of Cyclic Voltammetry. Because our system is symmetric in both the geometries of the positively/negatively charged pores and the structure of the cations/anions, we only discuss the charge storage in the positively charged pore. Figure 1 shows the first few cycles of the charging and discharging of a 0.78 nm wide pore at a representative scan rate of 5 V/ns. As voltage increases (decreases) (Figure 1a), counterions are inserted into (removed from) the pore, while the co-ions are removed from (inserted into) the pore (Figure 1b). Their responses to the applied voltage deviate from those in the quasi-static limit. While the insertion/removal of counterions is synchronized quite well with the evolution of the applied voltage, the response of co-ions lags significantly behind. Indeed, co-ions are removed from the pore well beyond the conclusion of the first forward scan; they start to be inserted into the pore only when the first backward scan is nearly finished (cf. the second vertical dashed line in Figure 1b), and their insertion terminates shortly after the second forward scan starts (cf. the fourth vertical dashed line in Figure 1b). These features, that is, prolonged removal of co-ions until the voltage is decreased to ∼1 V and quick termination of co-ion insertion once the voltage increases back to ∼1 V, are repeated in subsequent cycles. The response of counterions and co-ions to the cyclic voltage reaches a periodic steady state within about three cycles, in line with that observed in experimental studies.[7,8]

The different responses of counterions and co-ions to the applied voltage have both dynamic and thermodynamic origins. As described above, the flux of counterions inside of the pore is usually stronger than that of the co-ions because of their higher density. This phenomenon, along with the fact that the net flux of ionic species into/out of the pore is dominated by the transport of these species inside of the pore toward the pore

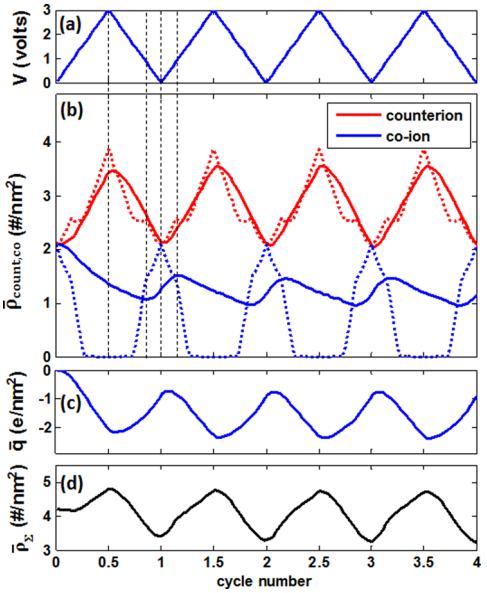

Figure 1. The first few cycles of the charging and discharging of a 0.78 nm-wide electrode pore at a scan rate of 5 V/ns. (a) Evolution of the half-cell voltage. (b−d) Evolution of the average counterion and co-ion densities ($\bar{\rho}_{count,co}$), charge density $\bar{q}$, and total ion density $\bar{\rho}_\Sigma$ inside the pore ($\bar{q} = \bar{\rho}_{co} - \bar{\rho}_{count}$; $\bar{\rho}_\Sigma = \bar{\rho}_{co} + \bar{\rho}_{count}$). In (b), the evolution of ion densities during quasi-static (infinitely slow) charging/discharging is shown as dotted lines. Densities are presented as area density as the ions confined in the pore form a single layer. The usage of ultra-fast scan rate in this and all other figures is justified because of the short length of the nanopores in our model system (see text for explanation).

interior/entrance, causes counterions to respond more effectively to the evolving voltage applied on the electrode than co-ions. This trend is especially pronounced at times when the density of counterions inside of the pore is already much larger than that of the co-ions. For example, Figure 1b shows that while the counterion's insertion rate is comparable to the co-ion's removal rate at the initial stage of the first forward scan, it soon exceeds the co-ion's removal rate as charging proceeds, that is, as the pore becomes populated by more counterions but fewer co-ions.

A consequence of the slow removal of co-ions from the pore during the first forward scan (the "charging" scan) is that co-ions continue to be removed from the pore during a significant portion of the first backward scan (the "discharging" scan). Specifically, at the end of the first forward scan, co-ions remain of high density inside of the pore, although from a thermodynamic perspective, the electrode polarization demands co-ions to be fully depleted (cf., the density of co-ions at the quasi-static condition in Figure 1b). Therefore, co-ions continue to be removed during the backward scan until the voltage on the electrode drops to ∼1 V, when the density of co-ions inside of the pore becomes comparable to that thermodynamically demanded by the voltage.

The different response of counterions and co-ions to the voltage cycling identified above leads to interesting phenomena. Because counterion insertion (removal) and co-ion removal (insertion) are generally not synchronized and their rates are also different, the cycling of the applied voltage leads to not only a cycling of the net charge inside of the pore (see Figure 1c) but also a cycling of the total ion density inside of the pore (see Figure 1d). The latter result indicates that the total mass of

dx.doi.org/10.1021/jz5024306 | J. Phys. Chem. Lett. 2015, 6, 22−30

a porous electrode changes periodically during charging/discharging, which has been reported experimentally and leveraged to study the mechanism of dynamic charge storage in nanoporous electrodes.[9] Another manifestation of the different counterion and co-ion dynamics is the non-neutral state of the pore each time the voltage returns to zero (hereafter termed the state of zero voltage). The introduced notion of the state of zero voltage (SZV) is fundamental for the cyclic charging and discharging of a nanopore. It defines the initial condition for each forward scan. As expected from the classical TLM,[25] for pores polarized by the voltage signal in Figure 1a, the net ionic charge inside of them is negative at each SZV. While TLM provides no information on the composition of the electrolyte inside of a pore,[26] Figure 1b and c shows that, compared to the PZC state, the SZV features a weak excess of counterions and a significant shortage of co-ions, that is, a reduced total ion density. It is worth noting that the lower total ion density at SZV compared to that at the PZC has been discovered by Richey et al. in the infrared spectroelectrochemical characterization of dynamic charge storage in microporous CDC electrodes (pore size: 0.85 nm) immersed in ionic liquids.[8] This interesting experimental observation may be related to the mechanisms delineated above.

Cyclic Charging/Discharging and the Underlying Ion Dynamics. We now examine the dynamic charge storage at periodic steady states, which is the focus of most cyclic voltammetry studies. Figure 2a shows that the computed cyclic voltammogram closely resembles those measured experimentally.[9] During quasi-static charging, the normalized current shows a peak in the 1−1.5 V voltage window during the forward scan, which is caused by the counter/co-ion demixing. Quasi-static discharging shows a symmetrical peak located in the 1−1.5 V range. In sharp contrast, these peaks disappear in cyclic voltammetry at a scan rate of 5 V/ns. Its difference from the quasi-static results gives a clear illustration of the effect of ion transport on the dynamic charge storage in nanopores.

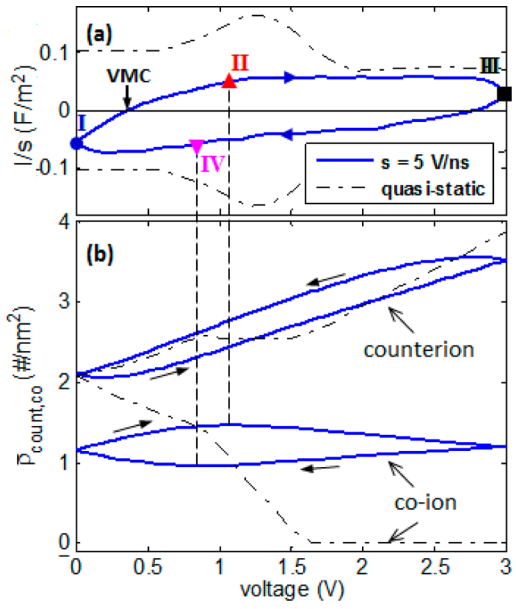

Figure 2. The evolution of current I normalized by scan rate s (panel a) and the average counter/co-ion densities inside the pore (panel b) during the steady-state charging/discharging cycles of a 0.78 nm-wide pore. The evolutions of normalized current and ion densities during the quasi-static charging/discharging are shown as dot-dashed lines. Points II and IV correspond to the voltages at which the net transport of co-ions reverses its direction. The voltage of minimal charge (VMC) is defined in the text.

To gain insights into what contributes to the charging and discharging currents quantified in Figure 2a, we study their underlying ion dynamics (see Figure 2b). As detailed above, at SZV, the number of counterions inside of the pore is nearly comparable to that at the PZC state, that is, that demanded thermodynamically by the electrode polarization. However, the number of co-ions inside of the pore is much less than that at the PZC. As such, at SZV, there is a large driving force for co-ions to enter into the pore, giving a negative current (point I in Figure 2a). As the voltage increases, the number of co-ions inside of the pore increases (Figure 2b), which favors counterion insertion and meanwhile hinders co-ion insertion. Consequently, co-ion insertion slows down, and counterion insertion speeds up; eventually, the current reaches zero at ∼0.38 V, where the magnitude of net charge inside of the pore reaches a minimum (this voltage is termed voltage of minimal charge, or VMC). Interestingly, until the voltage increases further to ∼1 V (point II in Figure 2a), counterions and co-ions are inserted concurrently into the pore (Figure 2b). The ion dynamics in the remainder of the forward scan is similar to that expected from the TLM.[25] However, the TLM cannot discern the effect that, at the end of the forward scan (point III in Figure 2a), both the counterion and the co-ion densities are higher than those at the beginning of the forward scan (Figure 2b). The significant accumulation of counterions is responsible for the energy storage during the charging stage. However, the net accumulation of co-ions during the forward scan indicates that they contribute *negatively* to charge storage (this effect becomes more pronounced as the scan rate increases; see Figure S4, Supporting Information). This phenomenon, unique to the fast and cyclic charging of narrow pores, is caused by the persistent insertion of co-ions into the pore until ∼1 V is reached and by the sluggish removal of co-ions thereafter. The former mostly originates from the large deficiency of co-ions at the SZV compared to that at the PZC.

The ion dynamics during the backward scan largely follow the expected behavior: as the voltage decreases, counterions are removed from the pore while more co-ions are supposed to enter the pore. However, the number of co-ions inside of the pore does not immediately increase as the backward scan starts. In fact, their number keeps decreasing until the voltage drops to ∼0.8 V (point IV in Figure 2b). The persistent but sluggish removal of co-ions over such a wide voltage window has similar origins as that observed during the backward scan in the first charging/discharging cycle (see Figure 1b). Afterward, the number of co-ions increases slightly until the SZV. In comparison, during the entire backward scan, the number of counterions decreases monotonically all the way to the SZV.

Overall, at the high scan rate considered here, both the charging during the forward scan and the discharging during the backward scan are dominated by the transport of counterions. The co-ions play a relatively limited role despite that they *do* participate in these processes. Their net contribution to charging is small as their transport during the two phases of the forward scan (I → II and II → III in Figure 2b) essentially cancels out each other (see Figure 2b). The same effect applies to discharging during the backward scan.

In the discussion thus far, all ions inside of the pore except those at the immediate entrance of the pore are treated in a lumped fashion. Such a treatment allows the net ion transport

dx.doi.org/10.1021/jz5024306 | J. Phys. Chem. Lett. 2015, 6, 22−30

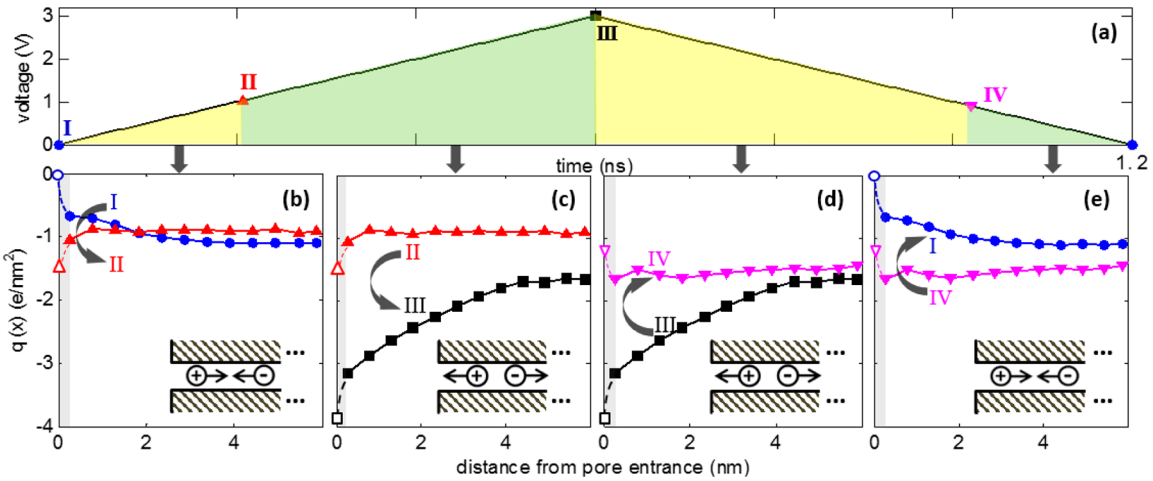

Figure 3. Evolution of the half-cell voltage (panel a) and the ionic space charge density profile inside the pore (panels b–e) during cyclic charging/discharging of a 0.78 nm-wide pore (scan rate: 5 V/ns). Points I–IV correspond to those in Figure 2a. As the pore is open at both ends, only the space charges between the pore entrance ($x = 0$) and the pore center are shown. The variation of the ionic space charge near $x = 0$ (shaded regions in b–e), too sharp to be resolved in MD simulations, is shown as dashed lines with the charge at the pore entrance taken as its quasi-static value (denoted by open symbols). Insets of panels b–e show the electrical migration of counterions and co-ions (represented by one anion and one cation in each carton) within the pore driven by electrostatic ion-ion interactions during different phases of a cyclic scan. The direction of these migrations is determined using the ionic space charge profile in b–e and eq 1. These migrations counteract the ion transport driven by the external voltage during phases I → II and III → IV; the opposite occurs during phases II → III and IV → I.

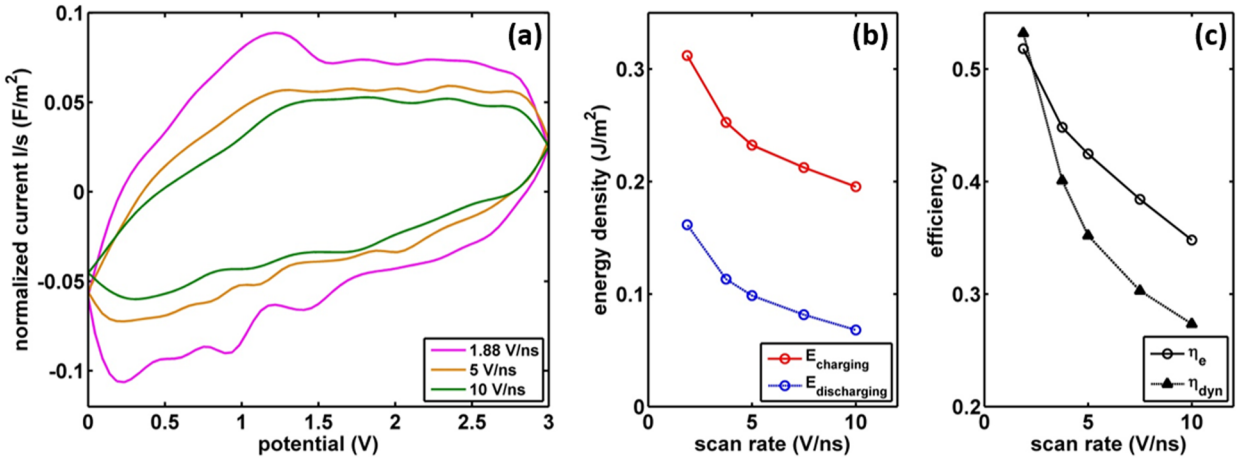

Figure 4. (a) Cyclic voltammograms of a 0.78 nm-wide pore operating at different scan rates. (b) Effects of scan rate on the energy needed for charging a 0.78 nm-wide pore ($E_{charging}$, see eq 2) and the energy released by the pore during discharging ($E_{discharging}$, see eq 3). (c) Effects of scan rate on the charge storage efficiency η_{dyn} and the energy storage efficiency η_e of the pore during cyclic charging and discharging.

into/out of the pore to be analyzed qualitatively without spatially resolving the ion transport inside of the pore. To scrutinize the ion dynamics during charging/discharging in greater detail, we next examine the internal ion transport in a spatially resolved manner. We focus only on the electrical migration of ions because it often dominates the overall charging/discharging behavoir.[11] Figure 3 shows the spatial-temporal evolution of the ionic space charge inside of the pore during the four phases of a voltage cycling (I → II, II → III, III → IV, and IV → I in Figure 2a). The evolution of the ionic charge profile in the pore interior exhibits a sloshing pattern. In the forward scan, the ionic charge profile is concave at point I; it becomes nearly flat at point II and convex at point III. The opposite pattern occurs during the backward scan. It is evident from eq 1 that such a sloshing of ionic charge drives ion transport within the pore: counterions (anions) migrate toward the pore entrance, and co-ions (cations) move toward the pore interior in phases I → II and IV → I, delivering negative charge toward the pore entrance; the opposite process occurs in phases II → III and III → IV (see insets of Figure 3b–e).

The net ion transport into/out of the pore is a result of the interplay between the ion transport induced by an applied voltage and by the internal sloshing of ionic charges. In the forward scan, the increase of electrode polarization tends to drive anions (counterions) into the pore and cations (co-ions) out of the pore. During phase I → II, the sloshing of ionic space charge inside of the pore delivers anions toward the pore entrance and cations toward the pore interior, thus counteracting the effect of the applied voltage. One can show that the sloshing of ionic space charge during phase III → IV has a similar effect but that during phases II → III and IV → I, it enhances the action of the applied voltage. The competition between the charge transport caused by the sloshing of ionic space charges and the applied voltage during phases I → II and

dx.doi.org/10.1021/jz5024306 | J. Phys. Chem. Lett. 2015, 6, 22–30

III → IV helps explain why the net ionic current during these phases is smaller than that during phases II → III and IV → I, in which the sloshing of ionic space charges and the applied voltage cooperate with each other.

Effects of Scan Rate and Pore Size on Dynamic Charge Storage. Figure 4a compares the cyclic voltammograms of a 0.78 nm wide pore operating at different scan rates. As the scan rate increases, the current deviates more and more from that at the quasi-static charging/discharging condition. In particular, the charging current at moderate voltages (0.5−1.2 V) decreases sharply with increasing scan rate, while at large voltages (>∼1.5 V), it decreases moderately. To quantify how the performance of the dynamic charge storage inside of the pore is affected by the scan rate, we compute the electrical energy needed to charge the pore during the forward scan $E_{charging}$, the energy delivered by the pore during the backward scan $E_{discharging}$, and the voltammetric charge Q_v by

$$E_{charging} = \int_0^{t_f} V(t)I(t)\,dt = \int_{\bar{q}(0)}^{\bar{q}(t_f)} V(\bar{q})\,d\bar{q} \quad (2)$$

$$E_{discharging} = \int_{t_f}^{t_b} V(t)I(t)\,dt = \int_{\bar{q}(t_f)}^{\bar{q}(t_b)} V(\bar{q})\,d\bar{q} \quad (3)$$

$$Q_v = \int_0^{t_f} I(t)\,dt = \int_{t_f}^{t_b} I(t)\,dt \quad (4)$$

where $t = 0$ is the starting time of a full scan. t_f and t_b are the time when the forward and backward scans ends, respectively. V, I, and $\bar{q}$ are the half-cell voltage, the net ionic current into/out of the pore, and the average charge inside of the pore. The energy efficiency of the charge storage, also called the watt−hour efficiency,[25] is computed using $\eta_e = E_{discharging}/E_{charging}$. The charge efficiency is computed using $\eta_{dyn} = Q_v/Q_{equ}$, where Q_{equ} is the amount of charge stored inside of the pore under quasi-static charging conditions. Note that η_{dyn} is different from the amp−hour (or Coulomb) efficiency,[25] which is 100% due to the absence of stray currents in our simulations.

Figure 4b shows that, as the scan rate increases, both the energy needed to charge the pore and the energy delivered by the pore during discharging decrease due to less charge being stored/released during the charging/discharging half cycle (Figure 4c). Figure 4c also shows that the overall energy efficiency of the charge storage/release cycle also decreases as the scan rate increases, which is consistent with the results shown in Figure 4a, that is, at high scan rates, most charges are stored at high voltage (thus requiring more energy; cf. eq 2) but released at low voltage (thus delivering less energy). Figure 4c further shows that the charge efficiency decreases with increasing scan rate. However, the pore still retains ∼30% of its charge storage capability at scan rate up to 10 V/ns. This indicates that while the scan rates in this study are far greater than those in common experimental studies, they can be used to probe the physics of dynamic charge storage in the nanoscopic systems considered here. This is akin to the fact that, although scan rate is limited to less than a few hundred mV/s in typical cyclic voltammetry experiments, scan rates up to several V/s can be used to characterize the charging dynamics of cavity microelectrodes.[27]

The response of $E_{charging}$, $E_{discharging}$, and η_e to the scan rate shown above originates from the fact that as the scan rate increases, the charging (discharging) current decreases, especially at low (high) voltages. This fact is consistent with the expectation that as the scan rate increases, counterions (co-ions) have less time to be inserted into (removed from) the pore, which is already predicted by the classical TLM. Close inspection of the ion dynamics underlying the cyclic charging and discharging, however, shows that the response of the charge storage to the scan rate exhibits unique features that are not described by the classical TLM.

The classical TLM does not distinguish the role of counter/co-ions in charging/discharging as ion density does not explicitly appear in the model. Hence, it cannot provide information on the relative contribution of counter/co-ions to dynamic charge storage. On the other hand, our simulations indicate that counterions dominate the dynamic charge storage, especially at high scan rates. Figure 5 shows how the average densities of counterions and co-ions inside of a pore vary as the pore becomes charged. The ion densities and net ionic charge are offset by their values at the VMC because the net charge inside of the pore is not zero at the beginning of the forward scan (cf. Figure 2a,b). Under quasi-static conditions, counterion insertion and co-ion removal contribute similarly to charge storage until the pore becomes moderately charged (∼1.2 e/nm^2); further charging is contributed almost solely by the removal of co-ions until they are completely removed, after which counterion insertion dominates charging (not shown). These different roles of counter/co-ions in charge storage are thermodynamic in origin, and their mechanisms have been previously clarified.[10,11,23,24] However, at finite scan rates, the contributions of counter/co-ions to charge storage changes greatly. At a scan rate of 1.88 V/ns, before $q - q_{VMC}$ reaches ∼1.2 e/nm^2, the contribution of counterion insertion and co-ion removal to net charge storage deviates moderately from those under quasi-static conditions. Specifically, counterions

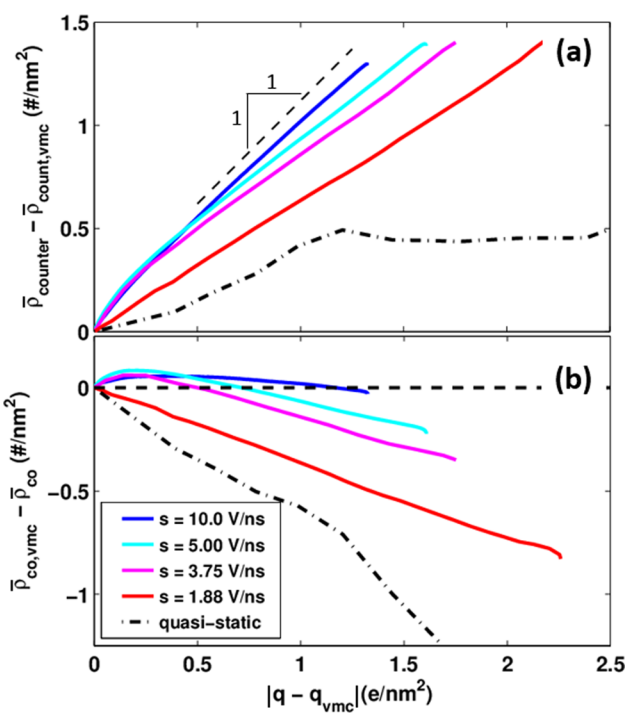

Figure 5. Variation of the average counterion (a) and co-ion (b) densities inside of a 0.78 nm wide pore during charging. The ion densities ($\rho_{count/co}$) and net ionic charge (q) are offset by their values at the VMC. In panel a, the thin dashed line corresponds to the situation in which charging is contributed solely by insertion of counterions.

dx.doi.org/10.1021/jz5024306 | J. Phys. Chem. Lett. 2015, 6, 22−30

contribute more while co-ions contribute less to the dynamic charge storage. As charging proceeds further, the relative contribution of counter/co-ions does not change greatly. This latter behavior, however, differs from that in the quasi-static charging, in which charging from $q - q_{VMC} = 1.2$ to 2.2 e/nm^2 is almost solely due to co-ion removal. As the scan rate further increases, the contribution of co-ions to the charge storage is further reduced, for example, at scan rates faster than 3.75 V/ns, co-ions are even inserted into the pore during the early stage of charging (Figure 5b), thus contributing negatively to net charge storage. As a result, charge storage is increasingly achieved through counterion insertion. Indeed, at a scan rate of 10 V/ns, charge storage is achieved almost exclusively through the insertion of counterions (cf. Figure 5a).

The ion dynamics exposed above resemble those observed in recent experiments. In particular, the dominance of charging by counterions is similar to that reported in the pioneering EQCM studies by Levi et al. and Tsai et al.[6,9] Both research groups found that under certain conditions, the charging of the pore is contributed almost solely by the insertion of counterions (termed perm-selectiveness). The perm-selectiveness observed by Levi et al.[6] seems to be thermodynamic in nature as charging was found to be independent of the scan rate when the perm-selectiveness was observed. The perm-selectiveness observed by Tsai et al.,[9] however, could have different origins. Specifically, for CDC electrodes (pore size: 1.0 nm) in contact with EMI-TFSI electrolytes, charge storage in the negative polarization (when the EMI^+ ion is the counterion) and in part in the positive polarization (when the $TFSI^-$ ion is the counterion) was found to be contributed solely by the insertion of counterions at a scan rate of 10 mV/s. Prior simulations of the charge storage in porous carbons with similar pore size and electrolytes show that, at equilibrium, the contributions of counterion insertion and co-ion removal to the net charge storage are quite similar.[19,24] Therefore, the perm-selectiveness observed in Tsai et al.'s study likely has dynamic origins similar to what was observed and discussed in detail above. Note that while a scan rate of 10 mV/s is relatively small, charging at this rate can still show dynamic effects. In fact, even at a scan rate of 0.5 mV/s, there can be incurrence of significant dynamic effects for some systems.[7]

The effect of pore size on charging and discharging was also examined. The result for a 0.91 nm wide pore exhibits similar features as that for the 0.78 nm wide pore discussed above. As shown in Figures S4–S6 (Supporting Information), the SZV of the pore is characterized by a deficiency of co-ions compared to the PZC state. In these cases, the dynamics of counterions follow more closely the evolution of the applied voltage, while co-ions lag behind; co-ions are inserted into the pore concurrently with counterions during the initial phase of the forward scan with high rates, while counterions dominate the charging of the pore at large scan rates. However, because the transport of ions is less sluggish than that in the 0.78 nm wide pore (cf. eq 1), the charging/discharging of this pore is more efficient (Figure S5c, Supporting Information). The response of counterions and co-ions to the applied voltage is less disparate compared to that in the 0.78 nm wide pores: the concurrent insertion of counter/co-ions terminates at smaller voltages compared to that in narrower pores. While counterions still dominate the charging, co-ions contribute notably to charging even at the highest scan rate examined here (cf. Figure S6, Supporting Information).

In summary, we have studied the cyclic charging and discharging of supercapacitors based on subnanometer pores and RTILs by using MD simulations. These simulations allowed us to probe the dynamic charge storage at the single-pore level both spatially and temporally, which is extremely difficult, if possible at all, to access experimentally. We found that the cyclic charging and discharging of a nanopore are governed by the external field-driven ion transport and the sloshing dynamics of ions inside of the pore. These two processes compete with (or facilitate) each other during the beginning (late) phase of the forward and the backward scan, which leads to the asymmetric shape of the cyclic voltammogram.

The dynamic charge storage in subnanometer pores is dominated by counterions, especially at high scan rates and in narrower pores. Such a phenomenon differs greatly from the charge storage under equilibrium conditions. The predominant contribution of counterions to the charge storage observed here, termed perm-selective charging by prior researchers, is caused by the stronger electrical migration flux of counterions during charging, which in turn is caused by the relative abundance of counterions over co-ions inside of the pore. As the pore becomes wider, the relative abundance of counterions over co-ions weakens, and therefore, the co-ions contribute more to charge storage, albeit still at a lesser degree than counterions.

Our simulations showed that during cyclic charging/discharging, nanopore systems are driven to far-from-equilibrium states. Indeed, the internal state of the nanopore (in particular, the total ion density) not only deviates from that under quasi-static charging/discharging conditions but also varies greatly as the scan rate changes. Because these phenomena affect the energy and charge storage efficiency of the cyclic charging/discharging of nanopores, they should be considered when developing improved theories for charging/discharging of supercapacitors.

In the present coarse-grained simulations, simplistic models are used for ions and pore walls, and the specific interactions between them are neglected. In practice, the specificities of ions and ion–wall interactions can affect the dynamics of charge storage in nanopores, for example, the specific adsorption of ions in pores can greatly affect their transport properties and thus the dynamic charge storage. Clarifying the effects of these specificities requires simulations resolved at quantum, molecular, and pore scales. Such multiscale simulations represent a grand challenge in materials modeling and cannot be achieved by brute-force coupling of the simulations at these scales. However, developing understanding of the generic features determined by collective interactions between the RTIL ions in a nanopore, screened by the electronic polarizability of the pore, is fundamental. This was the goal of the present work. We believe that its findings will provide a useful reference base for more sophisticated, multiscale simulations that will involve the detailed structure and chemical complexity of RTILs and electrode materials.

METHODS

The MD system consists of a pair of identical slit pores and two reservoirs separating the pores (Figures S1 and S2, Supporting Information). The length of each pore and each reservoir is 12.09 and 10.92 nm, respectively. Each pore wall is made of a square lattice of Lennard-Jones particles with an atom spacing of 0.17 nm. Each ion has identical geometry to the BF_4^- ion,

dx.doi.org/10.1021/jz5024306 | J. Phys. Chem. Lett. 2015, 6, 22–30

with its central atom carrying a unit positive or negative charge. The mass density of the model RTIL used in this work is 991 kg/m^3 (P = 1 atm, T = 400 K), which is within the range of RTIL density found experimentally (~900−1300 kg/m^3).[28] With the force fields used for ions and wall atoms, cation and anions form a single layer inside of each pore considered here (Figure S3, Supporting Information). A target potential V_{max} of 6 V is used because it is essential to understand the charge storage of RTILs at high voltages. While this potential is high, it is comparable to the electrochemical window of some RTILs, for example, *N*-methyl-*N*-butyl-pyrrolidinium bis-(trifluoromethanesulfonyl)-imide (5.5 V at 60 °C).[29] To determine the charging/discharging in the quasi-static limit, separate systems with 50% shorter pores and RTIL reservoirs were run for 20 ns to obtain the equilibrium charges inside of the pores when the voltage difference between the negative and positive pores are 0.3, 0.6, ..., 6 V. The integral capacitance is 10.3 and 9.41 μF/cm^2 for the 0.78 and 0.91 nm pores at V_{max} = 6 V, respectively, which is similar to the experimental value for subnanometer pores filled with RTILs.[30] The electrode potential of a pore is presented using the potential at the middle of the RTIL reservoir as a reference, and its change per unit time defines the scan rate.

Simulations were performed using a modified Gromacs code.[31] Prior studies have concluded that it is important that the charging of nanopores be simulated by enforcing a constant potential on each pore wall rather than assigning static charges to wall atoms.[32] Here, the electrical potential on the pore wall was enforced within the framework of continuum electrostatics:[33] each pore wall was modeled as an equipotential surface, with its image plane coinciding with the geometric plane of the wall atoms. This method has produced similar results compared to other methods for enforcing electrical potential on pore walls.[19,20,24] Simulations were performed in the *NVT* ensemble with T = 400 K. Such an elevated temperature helps increase the diffusion coefficient of the ions so that charging dynamics can be studied with the available computational resources. Specifically, the self-diffusion coefficient of ions in bulk RTILs under the same conditions as those in the RTIL reservoir was found to be $D_+ = D_- = 2.32 \times 10^{-9}$ m^2/s, which is ~1−2 order of magnitude larger than that of typical RTILs used in supercapacitors. Simulation at lower temperature is difficult because the diffusion of ionic liquids slows down greatly as the temperature reduces. Therefore, charging/discharging of the pores considered here (i.e., charge efficiency > 20%) will require a long simulation time (e.g., thousands of nanoseconds) and a prohibitive amount of computer time. During each simulation, the evolutions of cation and anion densities along each pore were computed on the fly. These data were used to compute the net charge inside of each pore, which was then used to compute the charging/discharging current, the energy stored (released) during the charging (discharging), and the energy efficiency of each charging/discharging cycle. Each cyclic voltammetry study was repeated three times with independent initial configurations. Further details such as the calculations of electrostatic forces are provided in the Supporting Information. A time step of 3 fs was used in production runs. Our tests indicated that in the *NVE* simulations of bulk RTILs based on our coarse-grained model, the energy drift was less than 0.2% over 10 ns when a time step of 3 fs was used. Such a relatively large time step is often used in coarse-grained MD simulations because some of the faster modes are no longer active due to coarse-graining.

■ ASSOCIATED CONTENT

Supporting Information

Schematic of the MD system, force field parameters, MD simulation details, and charge storage characteristics of a 0.78 nm wide pore at other scan rates and of a 0.91 nm wide pore. This material is available free of charge via the Internet at http://pubs.acs.org.

■ AUTHOR INFORMATION

Corresponding Author

*E-mail: ruiqiao@vt.edu.

Notes

The authors declare no competing financial interest.

■ ACKNOWLEDGMENTS

We thank the Clemson-CCIT and the ARC at Virginia Tech for generous allocation of computer time on the Palmetto cluster and the BlueRidge cluster, respectively. R.Q. acknowledges the support from NSF (CBET-1461842). R.Q. was partially supported by an appointment to the HERE program for faculty at the Oak Ridge National Laboratory (ORNL) administered by ORISE. J.H. and B.G.S. acknowledge support from the Center for Nanophase Materials Sciences, which is sponsored at ORNL by the Scientific User Facilities Division, Office of Basic Energy Sciences, U.S. Department of Energy. A.A.K. acknowledges the former support of EPSC, which helped to start cooperation with R.Q.

■ REFERENCES

(1) Conway, B. E. *Electrochemical capacitors: scientific fundamentals and technological applications* Kluwer: New York, 1999.
(2) Simon, P.; Gogotsi, Y. Materials for electrochemical capacitors. *Nat. Mater.* **2008**, *7*, 845−854.
(3) Simon, P.; Gogotsi, Y. Capacitive energy storage in nanostructured carbon electrolyte systems. *Acc. Chem. Res.* **2013**, *46*, 1094−1103.
(4) Brandt, A.; Pohlmann, S.; Varzi, A.; Balducci, A.; Passerini, S. Ionic liquids in supercapacitors. *MRS Bull.* **2013**, *38*, 554−559.
(5) Levi, M. D.; Salitra, G.; Levy, N.; Aurbach, D.; Maier, J. Application of a quartz-crystal microbalance to measure ionic fluxes in microporous carbons for energy storage. *Nat. Mater.* **2009**, *8*, 872−875.
(6) Levi, M. D.; Levy, N.; Sigalov, S.; Salitra, G.; Aurbach, D.; Maier, J. Electrochemical quartz crystal microbalance (EQCM) studies of ions and solvents insertion into highly porous activated carbons. *J. Am. Chem. Soc.* **2010**, *132*, 13220−13222.
(7) Wang, H.; Forse, A. C.; Griffin, J. M.; Trease, N. M.; Trognko, L.; Taberna, P.-L.; Simon, P.; Grey, C. P. In situ NMR spectroscopy of supercapacitors: Insight into the charge storage mechanism. *J. Am. Chem. Soc.* **2013**, *135*, 18968−18980.
(8) Richey, F. W.; Dyatkin, B.; Gogotsi, Y.; Elabd, Y. A. Ion dynamics in porous carbon electrodes in supercapacitors using in situ infrared spectroelectrochemistry. *J. Am. Chem. Soc.* **2013**, *135*, 12818−12826.
(9) Tsai, W.-Y.; Taberna, P.-L.; Simon, P. Electrochemical quartz crystal microbalance (EQCM) study of ion dynamics in nanoporous carbons. *J. Am. Chem. Soc.* **2014**, *136*, 8722−8728.
(10) Kondrat, S.; Kornyshev, A. A. Charging dynamics and optimization of nanoporous supercapacitors. *J. Phys. Chem. C* **2013**, *117*, 12399−12406.
(11) Kondrat, S.; Wu, P.; Qiao, R.; Kornyshev, A. A. Accelerating charging dynamics in subnanometre pores. *Nat. Mater.* **2014**, *13*, 387−393.
(12) Péan, C.; Merlet, C.; Rotenberg, B.; Madden, P. A.; Taberna, P.-L.; Daffos, B.; Salanne, M.; Simon, P. On the dynamics of charging in

nanoporous carbon-based supercapacitors. *ACS Nano* **2014**, *8*, 1576−1583.
(13) Lee, A. A.; Kondrat, S.; Oshanin, G.; Kornyshev, A. A. Charging dynamics of supercapacitors with narrow cylindrical nanopores. *Nanotechnology* **2014**, *25*, 315401.
(14) Yang, X.; Cheng, C.; Wang, Y.; Qiu, L.; Li, D. Liquid-mediated dense integration of graphene materials for compact capacitive energy storage. *Science* **2013**, *341*, 534−537.
(15) Lukatskaya, M. R.; Mashtalir, O.; Ren, C. E.; Agnese, Y. D.; Rozier, P.; Taberna, P.-L.; Naguib, M.; Simon, P.; Barsoum, M. W.; Gogotsi, Y. Cation intercalation and high volumetric capacitance of two-dimensional titanium carbide. *Science* **2013**, *341*, 1502−1505.
(16) Kondrat, S.; Kornyshev, A. A. Superionic state in double-layer capacitors with nanoporous electrodes. *J. Phys.: Condens. Matter* **2011**, *23*, 022201. Corrigendum: **2013**, *25*, 119501.
(17) Shim, Y.; Kim, H. J. Nanoporous carbon supercapacitors in an ionic liquid: A computer simulation study. *ACS Nano* **2010**, *4*, 2345−2355.
(18) Skinner, B.; Chen, T.; Loth, M. S.; Shklovskii, B. I. Theory of volumetric capacitance of an electric double-layer supercapacitor. *Phys. Rev. E* **2011**, *83*, 056102.
(19) Merlet, C.; Rotenberg, B.; Madden, P. A.; Taberna, P.-L.; Simon, P.; Gogotsi, Y.; Salanne, M. On the molecular origin of supercapacitance in nanoporous carbon electrodes. *Nat. Mater.* **2012**, *11*, 306−309.
(20) Wu, P.; Huang, J.; Meunier, V.; Sumpter, B. G.; Qiao, R. Complex capacitance scaling in ionic liquids-filled nanopores. *ACS Nano* **2011**, *5*, 9044−9051.
(21) Jiang, D. E.; Jin, Z. H.; Wu, J. Z. Oscillation of capacitance inside nanopores. *Nano Lett.* **2011**, *11*, 5373−5377.
(22) Feng, G.; Cummings, P. T. Supercapacitor capacitance exhibits oscillatory behavior as a function of nanopore size. *J. Phys. Chem. Lett.* **2011**, *2*, 2859−2864.
(23) Wu, P.; Huang, J. S.; Meunier, V.; Sumpter, B. G.; Qiao, R. Voltage dependent charge storage modes and capacity in sub-nanometre pores. *J. Phys. Chem. Lett.* **2012**, *3*, 1732−1737.
(24) Xing, L.; Vatamanu, J.; Borodin, O.; Bedrov, D. On the atomistic nature of capacitance enhancement generated by ionic liquid electrolyte confined in subnanometre pores. *J. Phys. Chem. Lett.* **2013**, *4*, 132−140.
(25) Pell, W. G.; Conway, B. E. Voltammetry at a de Levie brush electrode as a model for electrochemical supercapacitor behavior. *J. Electroanal. Chem.* **2001**, *500*, 121−133.
(26) Within the classical TLM, the dynamic state of a pore is characterized by a *single* variable, that is, the distribution of the net charge along the pore.
(27) Lin, R.; Huang, P.; Ségalini, J.; Largeot, C.; Taberna, P. L.; Chmiol, J.; Gogotsi, Y.; Simon, P. Solvent effect on the ion adsorption from ionic liquid electrolyte into sub-nanometre carbon pores. *Electrochim. Acta* **2009**, *54*, 7025−7032.
(28) Zhang, S.; Sun, N.; He, X.; Lu, X.; Zhang, X. Physical properties of ionic liquids: database and evaluation. *J. Phys. Chem. Ref. Data* **2006**, *35*, 1475−1517.
(29) Arbizzani, C.; Biso, M.; Cericola, D.; Lazzari, M.; Soavi, F.; Mastragostino, M. High-energy supercapacitors based on solvent-free ionic liquid electrolytes. *J. Power Sources* **2008**, *185*, 1575−1579.
(30) Largeot, C.; Portet, C.; Chmiola, J.; Taberna, P.-L.; Gogotsi, Y.; Simon, P. Relation between the ion size and pore size for an electric double-layer capacitor. *J. Am. Chem. Soc.* **2008**, *130*, 2730−2731.
(31) Lindahl, E.; Hess, B.; van der Spoel, D. Gromacs 3.0: A package for molecular simulation and trajectory analysis. *J. Mol. Model.* **2001**, *7*, 306−317.
(32) Merlet, C.; Péan, C.; Rotenberg, B.; Madden, P. A.; Simon, P.; Salanne, M. Simulating supercapacitors: Can we model electrodes as constant charge surfaces? *J. Phys. Chem. Lett.* **2013**, *4*, 264−268.
(33) Raghunathan, A. V.; Aluru, N. R. Self-consistent molecular dynamics formulation for electric-field-mediated electrolyte transport through nanochannels. *Phys. Rev. E* **2007**, *76*, 011202.